Available online at www.sciencedirect.com

ScienceDirect

Journal of Magnesium and Alloys 9 (2021) 1753–1767

www.elsevier.com/locate/jma

Full Length Article

High temperature tensile, compression and creep behavior of recycled short carbon fibre reinforced AZ91 magnesium alloy fabricated by a high shearing dispersion technique

Sinan Kandemir[a,*], Sarkis Gavras[b,c], Hajo Dieringa[b,d]

[a] Department of Mechanical Engineering, Izmir Institute of Technology, 35430, Urla, Izmir, Turkey
[b] Helmholtz-Zentrum Hereon, MagIC – Magnesium Innovation Centre, Max-Planck-Straße 1, 21502, Geesthacht, Germany
[c] Helmholtz-Zentrum Hereon, Institute of Metallic Biomaterials, Max-Planck-Straße 1, 21502, Geesthacht, Germany
[d] Helmholtz-Zentrum Hereon, Institute of Materials and Process Design, Max-Planck-Straße 1, 21502, Geesthacht, Germany

Received 27 August 2020; received in revised form 14 March 2021; accepted 30 March 2021
Available online 15 May 2021

Abstract

The present study seeks the feasibility of using short carbon fibres recycled from polymer matrix composites as alternative to virgin carbon fibres in the reinforcement of magnesium alloys. The microstructures, high temperature mechanical and creep properties of AZ91 alloy and its composites with various recycled carbon fibre contents (2.5 and 5 wt.%) and lengths (100 and 500 μm) were investigated in the temperature range of 25–200 °C. The microstructural characterization showed that the high shear dispersion technique provided the cast composites with finer grains and relatively homogenous distribution of fibres. The materials tested displayed different behaviour depending on the type of loading. In general, while enhancements in the mechanical properties of composites is attributed to the load bearing and grain refinement effects of fibres, the fluctuations in the properties were discussed on the basis of porosity formation, relatively high reinforcement content leading to fibre clustering and interlayer found between the matrix and reinforcement compared to those of AZ91 alloy. The compressive creep tests revealed similar or higher minimum creep rates in the recycled carbon fibre reinforced AZ91 in comparison to the unreinforced AZ91.

Keywords: Metal matrix composites; Magnesium alloys; Recycled carbon fibre; High-shear dispersion; Microstructure; Mechanical properties; Creep.

1. Introduction

As one of the lightest structural metals, magnesium (Mg) and its alloys have attracted tremendous attention over the last few decades in many sectors such as the automotive sector where weight saving is a crucial factor for energy efficiency. Apart from high strength-to-weight ratio, they also offer high impact resistance, good castability and machinability [1–3]. However, Mg has some drawbacks including limited toughness and poor corrosion resistance, as compared to steel and aluminium. However, conventional Mg alloys exist which combine good room temperature strength and ductility with enhanced corrosion resistance in the market, e.g. aluminium-zinc (AZ60, AZ91) and aluminium-manganese (AM50, AM60). Note, the main alloying element in such alloys is aluminium for improving castability which is desirable for the manufacturing of complex shaped engineering components in larger scales with lower costs. It has been reported that approximately 90% of Mg-based automotive components including fuel tank covers, steering wheels and columns that are designed to function at room temperature are produced from the aforementioned alloys [4]. However, these alloys are far from providing required strength for powertrain applications subjected to elevated temperatures, such as gearbox housings. The reason behind the poor high temperature

* Corresponding author.
E-mail address: sinankandemir@iyte.edu.tr (S. Kandemir).

https://doi.org/10.1016/j.jma.2021.03.029

strength is commonly attributed to the presence of aluminium, resulting in the formation of $Mg_{17}Al_{12}$ β-phase which has poor thermal stability [5]. In addition, it is known that the majority of commercial Mg alloys exhibit poor creep resistance at temperatures above 127 °C [6].

In order to improve high temperature creep properties, hence widen the range for applications of Mg alloys, a number of approaches based on grain boundary reinforcement, solid solution and precipitation strengthening mechanisms have been proposed [7]. These approaches may be simply classified into two main groups: (1) alloy development and (2) introduction of micron or nano-sized reinforcements into monolithic Mg alloys, which promotes metal matrix composite (MMC) technologies. In alloy development, the use of rare earth elements is often required to precipitate thermodynamically stable compounds into Mg matrices [8–10]. However, the availability, supply risk and high cost of rare earth elements are considered the main issues in this approach. This led to further advancements in the field of Mg-based MMCs. The studies in such composites focused on using micron-sized ceramic particulates such as SiC, TiC and Al_2O_3, whiskers and fibres as reinforcements, and it was shown that some of them have satisfactory creep resistance at temperatures up to 250 °C [11–14].

There has been a recent attention focused on the development of Mg matrix nanocomposites reinforced with nano-sized ceramic particles and carbon nanotubes with less than 100 nm average diameter [15,16]. Such reinforcing elements have helped to further enhance mechanical properties and creep resistance of Mg alloys by stimulating grain refining and Orowan strengthening (dislocations bowing around reinforcement). However, there are still some challenges regarding the adaptation of these recently emerged nanocomposites into industrial application [4,17–19]. The first challenge is to obtain uniform dispersion and distribution of nano-sized reinforcements throughout the matrix for effective strengthening due to their large surface energy and low wettability in case of solidification processes. The second challenge is the potential harmful effect and health risks of using nanoparticles as the effects of nanoparticles on human body have not been entirely revealed yet [20]. It could be envisioned that nano-sized reinforcements may cause serious human health problems during both the nanocomposite fabrication processes and service in case of their disintegration from the matrix as a result of nanocomposite component failure.

Considering the drawbacks of Mg matrix nanocomposites, one method could be the further development of Mg matrix composites with micron-sized reinforcements, e.g. optimising constituents and processing parameters, in order to offer high creep resistant Mg-based materials with reasonable costs. Nowadays, carbon fibre reinforced plastics (CFRPs) are increasingly used in the aerospace and wind energy industries for weight savings. For this reason, it is important to recycle CFRPs from the end-of-life products for reducing their waste in terms of environmental and sustainable manufacturing. It has been proposed to reuse recycled carbon fibres (rCFs) which are extracted from polymers by various techniques including thermo-oxidation, pyrolysis and solvolysis, in order to fabricate composites for the automotive industry [21–23]. It was reported in numerous studies that the rCFs, which are environmentally friendly and considerably less costly compared with virgin carbon fibres (vCFs), have been successfully incorporated into polymeric matrices [24,25]. The short CFs which will be chopped off from long and continuous rCFs can be reused for reinforcing metals as well. It is considered that replacing vCFs which have already proven their effectiveness in improving high temperature mechanical properties of Mg alloys with low cost rCFs as reinforcement can introduce a new class of eco-friendly Mg composites into the market.

To the best of our knowledge, open literature sources so far suggested that there are only a few attempts reported for the use of rCFs in the Mg matrix composites fabricated by only solid state routes [26]. However, no study was conducted to incorporate rCFs into liquid Mg matrices and determine their creep properties. Therefore, a brief review of the literature on Mg matrix composites reinforced with only short vCFs is covered here. Ajukumar et al. [27] managed to obtain a distribution of short CFs into liquid AZ91 alloy with a good interfacial bonding by stir casting method, and found that the strength increases with increasing fibre content. Feldhoff [28] investigated the structure and chemistry of AZ91 matrix-CF interface and suggested that the plate-shaped carbide precipitates could be formed due to the chemical reaction between the carbon and liquid Mg-Al matrix. This is expected to alter the strength of matrix-fibre bonding, and hence affect the mechanical properties of composites. The first systematic attempt was made by Kainer [29] to determine the creep properties of Mg matrix composites reinforced with short CFs. In that study, AZ91/20 vol.% CF composites were fabricated by squeeze casting and it was reported that the composites exhibited enhanced elevated temperature strength and significant creep resistance compared to the monolithic alloy. The creep rate at 200 °C and 60 MPa was reduced from 6.3×10^{-7} to 2.6×10^{-9} s^{-1} with the addition of 20 vol.% CFs. Similar trends were also observed for the creep behaviour of AS41 alloy reinforced with 18 vol.% CFs [30].

The present study is aimed at determining the feasibility of using short rCFs as an alternative to their virgin counterparts in the fabrication of Mg matrix composites and investigating their potential effect on the microstructure and mechanical properties including creep resistance of the fabricated composites. Therefore, the developed fabrication technique is described here and the measured material properties are discussed along with the observed microstructures for both unreinforced matrix alloy and composites.

2. Experimental procedure

2.1. Materials

AZ91 alloy, which is utilized for the production of majority of Mg cast components in industry due to their excellent castability and good mechanical properties, was chosen as the matrix material. Its chemical composition was deter-

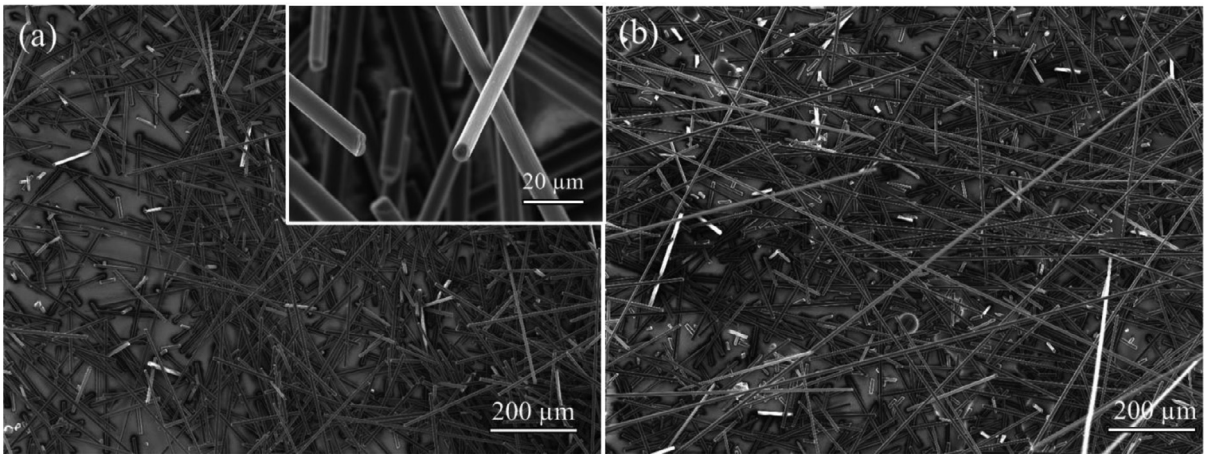

Fig. 1. SEM images of (a) rCF100 and (b) rCF500 as-received recycled carbon fibres.

Table 1
Chemical composition of AZ91 alloy (wt.%).

Mg	Al	Zn	Mn	Nd	Si	Ca	Cu	Fe
Bal.	8.73	0.67	0.21	0.019	0.019	0.0014	0.0027	0.0013

Table 2
Properties of rCFs from polymer matrix composites.

Carbon fibre content	95%
Tensile strength	>3500 MPa
Tensile modulus	>230 MPa
Fibre diameter	6 μm ($\pm$1 μm)
Density	1.83 g/cm^3
Sizing content	0%
Average fibre length	100 / >500 μm
Bulk density	>150 g/l

mined by a spark spectrometer (Ametek-Spectro, Spectrolab M9) and is shown in Table 1. For the reinforcement, two different rCFs in 100 and 500 µm average length were used (rCF100 and rCF500). The properties of rCFs supplied by CarboNXT Company, Germany, are given in Table 2 and their scanning electron microscopy (SEM) micrographs are presented in Fig. 1 (Details of the recycling process can be found at https://www.carbonxt.de/en/quality/). Prior to the introduction of rCFs into the matrix, they were exposed to a heat treatment of 400 °C in a furnace for an hour in order to burn away any polymer remnants that may be left from the recycling process and remove any absorbed gases, which may decrease the wettability between the rCFs and liquid Mg [31]. In the composite fabrication, the required amount of rCFs was introduced into the melt in aluminium foil bags in order to avoid their undesirable spread into air during handling and mixing operations.

2.2. Composite fabrication

Approximately 13 kg of commercial AZ91 molten alloy was placed into a steel crucible and held at 710 °C under a protective gas of Ar/1% SF_6. 2.5 and 5 wt.% rCFs in aluminium foil bags were introduced into the melt and the melt

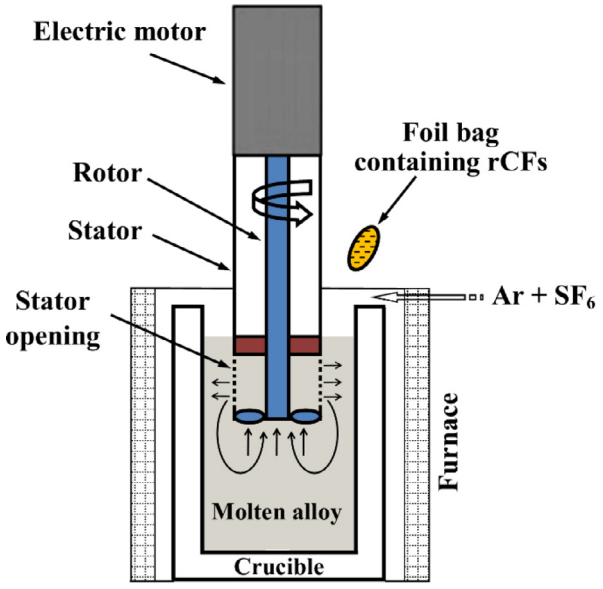

Fig. 2. Schematic experimental arrangement for high shearing dispersion process of rCFs.

was sheared for 5 min at 2000 rpm by a high shear dispersion device (Zyomax Ltd.) that was previously heated to 350 °C. This device is known to be more effective than mechanical stirrers in terms of generating required energy to deagglomerate potential particle or fibre agglomerations and it has been reported that the high shearing dispersion technique leads to microstructural refinement and reasonable dispersion of nanoparticles into various Mg alloys [32–34]. Further information about the device and technique can be found elsewhere [34]. The schematic experimental setup for composite fabrication is illustrated in Fig. 2. When the device composed of an open cylinder stator and motor driven rotor with a propeller is activated into the molten alloy, a reasonable quantity of melt is sucked into the stator and sheared and pushed inside the stator opening/holes. Thus, intensive shearing, in other words a high dispersion rate, can be achieved to facilitate deagglomeration of fibres. After the dispersion process, the molten composite was cast into cylindrical steel

molds with 100 mm diameter and 200 mm height preheated to 500 °C. Each mould containing about 3 kg liquid composite at around 670 °C was then placed into a water bath at a speed of 100 mm/min to secure controlled solidification conditions. For comparison, the reference alloy without the addition of rCFs was also cast under similar conditions. In total, five sets of cast samples were produced. These are reference AZ91 alloy, AZ91/2.5 wt.%rCF100, AZ91/2.5 wt.%rCF500, AZ91/5 wt.%rCF100 and AZ91/5 wt.%rCF500 composites.

2.3. Microstructural characterization and mechanical testing

The microstructures were investigated with an optical microscope (Leica DMI5000) and SEM (Tescan Vega 3 and Zeiss Evo 10) backscattered electron (BSE) imaging and secondary electron (SE) modes and energy dispersive X-ray (EDX) spectrometry. The samples were ground with abrasive papers ranging from 500 to 2500 grit size and polished with water-free 1 μm colloidal silica (OPS) and 1 μm diamond suspension. They were then exposed to etching with a solution of 15 ml distilled water, 140 ml ethanol, 6.5 ml acetic acid and 8 g picric acid for only optical microscopy. The average sizes of grains revealed and the densities of cast samples were measured based on linear intercept method and Archimedes' principle, respectively. X-ray diffraction (XRD) was carried out for the phase identification of samples with the following diffractometer parameters: Cu K_α radiation with a wavelength of 0.15418 nm, step scanning 2θ from 20° to 90° with a step size of 0.02°, 40 kV and 40 mA operating voltage and current, respectively.

Vickers hardness (HV) testing was conducted with a load of 5 kgf for 30 s. Ten indentations were made on each sample and the average data was presented. For mechanical testing, dog-bone shaped tensile (based on DIN 50143 and 50144 standards, in 6 mm gauge diameter and 30 mm gauge length), compression (9 mm diameter and 13.5 mm height) and compression creep (6 mm diameter and 15 mm height) specimens were machined from each set of cast cylinders. The tensile and compression tests were performed with a strain rate of 10^{-3} s^{-1} using a Zwick Z050 universal testing machine at room temperature (RT), 150, 175 and 200 °C. At least three specimens were tested for each set of specimens and test temperature, and average values were reported. The compression creep tests were carried out at 150 °C, 175 °C and 200 °C under constant compressive stresses between 50 and 120 MPa. ATS lever arm creep test machines were used in which the samples were kept at a constant temperature with a temperature deviation of ±1 °C controlled by two thermocouples. The deformation was recorded as a function of time.

3. Results and discussion

3.1. Microstructural characterization

Fig. 3 compares the polarized optical images of reference AZ91 alloy and its composites with rCFs from the middle sections in the cast blocks of each sample. As seen, the introduction of rCFs into AZ91 alloy significantly refined the microstructure and led to the reduction in grain sizes. The measured average grain sizes are given along with the porosity rates which were determined from the theoretical and measured densities of samples in Fig. 4a and b, respectively (The measured densities are given in Table 3). It can be suggested that there are no considerable effects of fibre content and length on the average grain sizes. It is also seen that the porosity rate tended to increase with the additions of rCFs, but the composites showed the divergent porosity rates ranging from 1.0% to 1.7%. This increased porosity level for the composites may be due to the possible air entrapment in the molten metal during the fibre feeding.

Table 3
Hardness test results and density measurements of the cast reference alloy and composites.

Sample	Hardness (HV)	Density (g/cm^3)
AZ91	55.5 ± 2.9	1.818
AZ91/2.5 wt.% rCF100	58.4 ± 5.6	1.807
AZ91/2.5 wt.% rCF500	59.9 ± 2.2	1.817
AZ91/5.0 wt.% rCF100	64.7 ± 3.0	1.818
AZ91/5.0 wt.% rCF500	61.1 ± 4.2	1.804

The SEM micrographs of the AZ91 alloy and rCF reinforced composites in BSE mode are presented in Fig. 5. It is observed that the rCFs were dispersed and distributed into the matrix both vertically and horizontally, showing no preferential orientation into the alloy. In addition, their distribution into the matrix is relatively uniform without significant casting defects and noticeable clusters except for the AZ91/5 wt.%rCF500 composite (Fig. 5e). The microstructure of this composite exhibits a few rCF agglomerates and this implies that the high shear dispersion technique is quite effective in terms of deagglomerating the vast majority of such micron-sized fibres. As shown in Fig. 6, the EDX elemental mapping analysis performed on a selected region of the AZ91/2.5 wt.%rCF100 composite confirms that the rCFs (C map) were embedded into the primary α-Mg grains and secondary β phase (mainly consists of $Mg_{17}Al_{12}$ intermetallic) precipitating along the grain boundaries. A single fibre embedded into an α-Mg grain that is marked on the SEM image in Fig. 6 has been further investigated by EDX analysis in order to detect any chemical reaction which could have taken place between the reinforcement and matrix as shown in Fig. 7. It is known that carbonaceous reinforcements are most likely to react with liquid Al forming brittle and undesirable Al_4C_3 phase at the interface. Although the single fibre was incorporated into a primary α-Mg grain containing no Al, the fibre-Mg interface, i.e. the surrounding of the fibre, displays considerable Al concentration as seen in the Al map (Fig. 7). This segregation on the fibre surface may be ascribed to the accumulation of Al, as the main alloying element, at the solidification front due to the temperature difference between the fibres and liquid alloy during the composite fabrication. The formation of an intermediate layer due to the reaction between the rCFs and liquid Al in the alloy would gener-

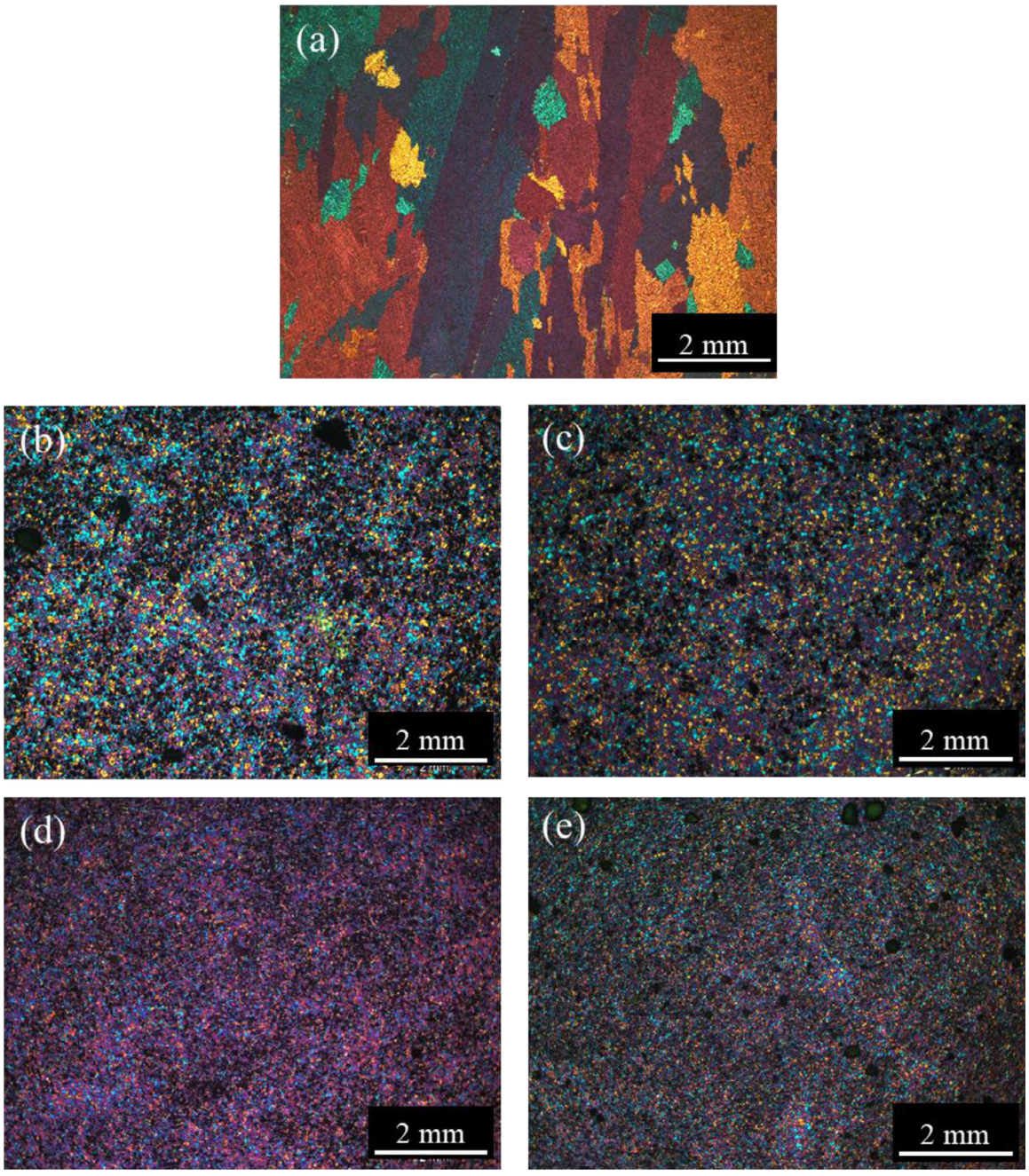

Fig. 3. Optical micrographs of (a) reference AZ91 alloy, (b) AZ91/2.5 wt.%rCF100, (c) AZ91/2.5 wt.%rCF500, (d) AZ91/5 wt.%rCF100 and (e) AZ91/5 wt.%rCF500 composite.

ate a stress concentration, which is expected to weaken the interfacial bonding, hence the mechanical properties [35].

It seems that there is an oxide formation around the single fibre as noticed in Fig. 7. Along with this oxide formation in the vicinity of reinforcement, a number of oxygen rich areas were also detected in all composite microstructures and a representative SEM micrograph of such areas with the EDX analysis is given in Fig. 8. This may suggest that considerable oxidation occurred during the composite fabrication despite the use of protective gas. Furthermore, the performed XRD analyses of the reference alloy and composites indicate the general phase identification containing α-Mg solid solution and β phase ($Mg_{17}Al_{12}$) and carbon in Fig. 9. Several investigations [36-39] reported that apart from the Mg and $Mg_{17}Al_{12}$ phases the carbides such as Al_4C_3 and Al_2MgC_2 being the reaction products were also observed in XRD analyses for the incorporation of carbonaceous reinforcements into molten Mg-Al alloys. Alongside with the formation of Al_4C_3 as discussed earlier, it was shown that Al_2MgC_2 can be formed at the CF-matrix interface for Mg alloys containing Al at a concentration between 0.6 and 19 wt.% [40]. However, those carbide phases cannot be identified by XRD in these AZ91 matrix

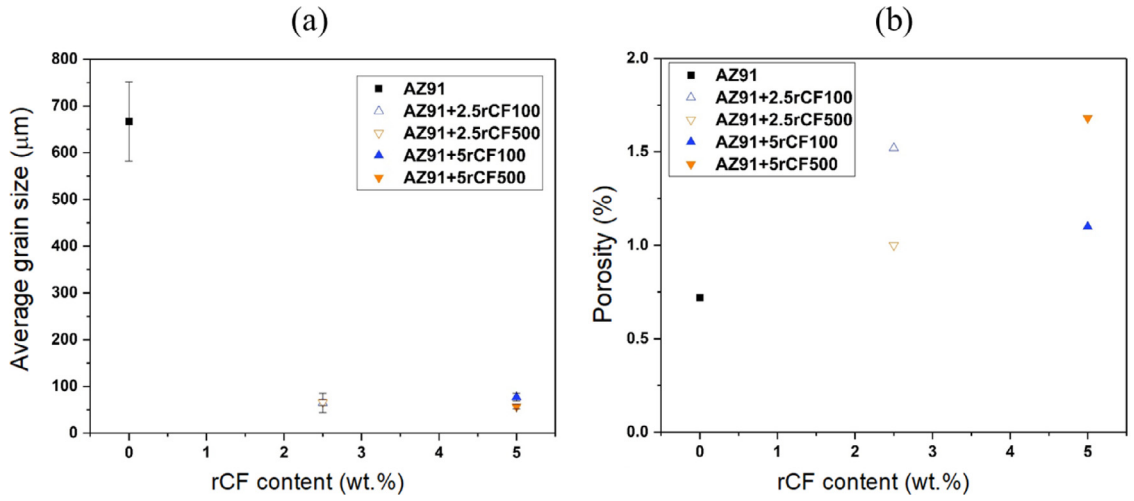

Fig. 4. Average grain sizes (a) and porosity rates (b) of the reference AZ91 alloy and composites with various rCF contents and lengths.

composites in spite of following a delicate sample preparation with water-free based agents as they are highly reactive with water. The main reason for not observing the potential peaks of Al_4C_3 and Al_2MgC_2 is likely to be their relatively lower content in the composites, which is likely to be less than the detection level of the XRD device. Nevertheless, the use of high resolution transmission electron microscopy is further suggested to precisely identify the intermediate phase found on the surface of rCFs embedded into AZ91 alloy as shown in Fig. 7.

3.2. Hardness

The hardness measurement results for the reference alloys and composites with different rCF additions are presented in Table 3 and these show an increase of approximately 5–8% and 10–16% in hardness of AZ91 with 2.5 and 5 wt.% rCF contents, respectively. As seen, the hardness is increased with increasing reinforcement addition due to the hardening effect of CFs limiting the local deformation, but the hardness enhancement is considered to be limited. Also, it is observed that there is no substantial effect of fibre length on the hardness values of composites containing 2.5 wt.% rCF. On the other hand, the shorter rCFs in 100 μm length displayed a noticeable hardness increment compared to the longer rCFs in 500 μm length for 5 wt.% rCF addition. This difference and limited hardness enhancement in all composites are consistent with the reported porosity rates in Fig. 4, and they can be therefore attributed to the increased amount of casting defects with reinforcement additions.

3.3. Tensile and compressive strength

The tensile and compressive properties including the average values of 0.2% proof stress (PS), ultimate tensile strength (UTS), ultimate compressive strength (UCS) and failure strain for the reference alloy and composites reinforced with rCFs at various temperatures are listed in Tables 4 and 5, respectively. In addition to the average test data, the representative tensile and compressive engineering stress versus strain curves of samples for RT, 150, 175 and 200 °C are given in Figs. 10 and 11, respectively. It can be observed from the average tensile test results that the 0.2% PS increased by between 9 and 23% with the incorporation of rCFs into AZ91 alloy, while the UTS and ductility decreased by 12–20% and 58–75%, respectively, depending on the fibre content and length at ambient conditions. In addition, the strength values tend to decrease, and ductility tends to rise with elevating temperature for all samples as expected since $Mg_{17}Al_{12}$ intermetallic begins softening at temperatures above 100 °C. Despite the divergent outcomes, the trend, in which the composites usually have greater PS values and reduced UTS and ductility compared to the unreinforced alloy with a few exceptions, is also observed to continue over the entire temperature range. It is well established that the strength enhancement in composites reinforced with micron-sized constituents is predominantly originated from load bearing and grain size reduction by the reinforcement, and increased dislocation density due to the mismatch in coefficient of thermal expansion between the matrix and reinforcement upon solidification. However, the reduction in UTS and ductility results of composites, which is also consistent with the previously reported studies [41,42], in principle, can be primarily ascribed to the porosity formation and the presence of relatively higher reinforcement content since the incorporation of more fibres inferring more clusters can induce large amount of pores as shown in Figs. 4 and 5e. Another explanation for the weakened properties could be given based on the formation of a relatively thick reaction layer at the rCF-matrix interface (Fig. 7) as potential structural damages (flaws or notches) led by the uneven chemical attack on the fibre surfaces is likely to impair the load bearing capacity of composites [43,44].

The effect of fibre content on both the PS and UTS was not found to be significant for all test temperatures as the composites with 2.5 and 5 wt.% rCFs showed comparable values with a margin of around 10%. This limited strength

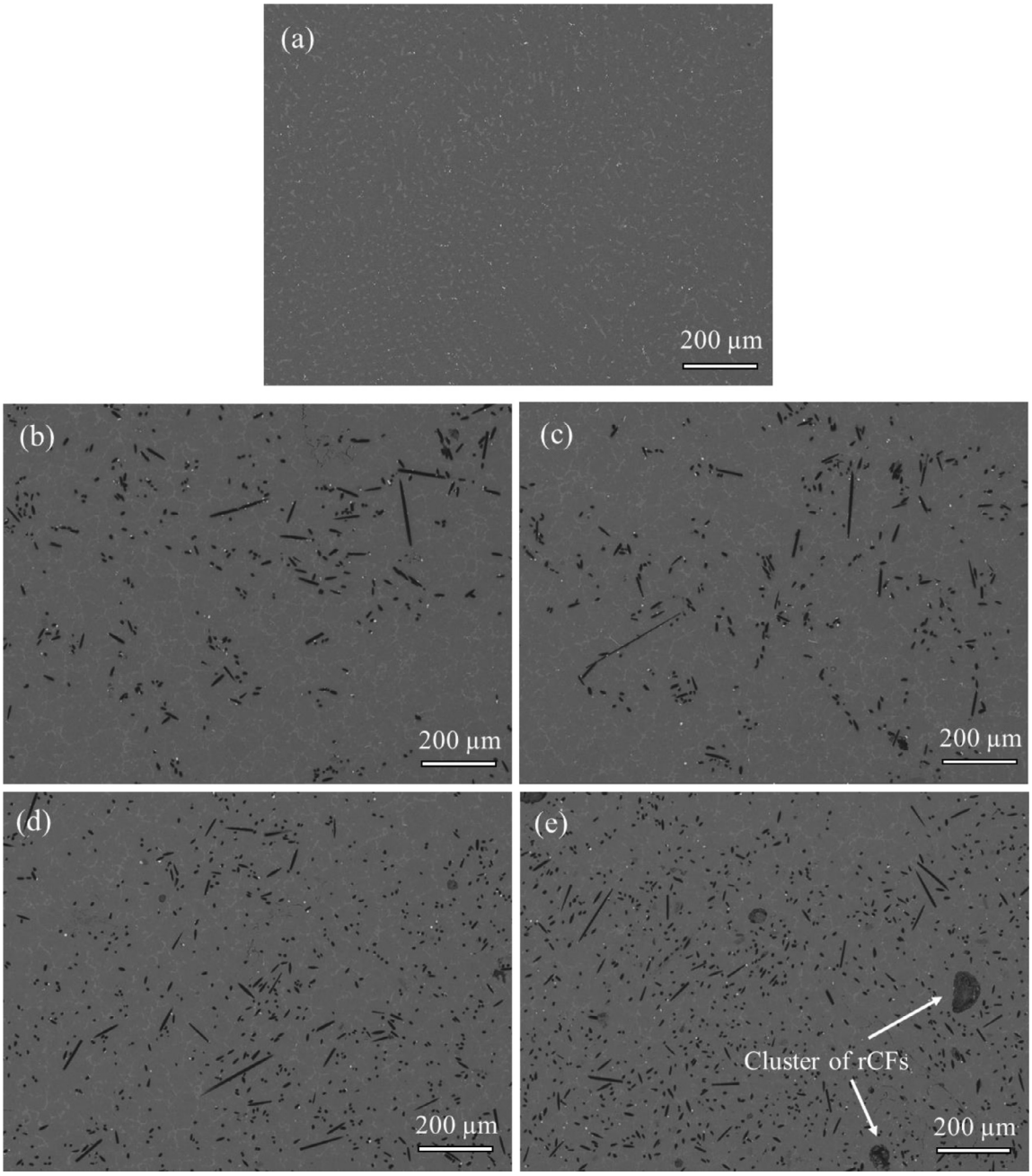

Fig. 5. SEM images of (a) reference AZ91 alloy, (b) AZ91/2.5 wt.%rCF100, (c) AZ91/2.5 wt.%rCF500, (d) AZ91/5 wt.%rCF100 and (e) AZ91/5 wt.%rCF500 composites.

Table 4
Tensile properties of cast AZ91 alloy and its composites reinforced with rCFs at different test temperatures.

	0.2% PS (MPa)				UTS (MPa)				Failure strain (%)			
Sample /test temperature	RT	150 °C	175 °C	200 °C	RT	150 °C	175 °C	200 °C	RT	150 °C	175 °C	200 °C
AZ91	87±12	93±17	82±14	70±5.7	165±14	166±13	146±7	112±4	2.4 ± 0.3	6.1 ± 4	5.1 ± 3.7	3.7 ± 0.9
AZ91/2.5 wt.%rCF100	95±2.8	93±5	80±2.7	74±5	132±13	128±10	126±5	106±7	0.8 ± 0.2	1.6 ± 0.7	2.6 ± 0.8	2.3 ± 1
AZ91/2.5 wt.% rCF500	107±7	101±9	78±6.5	81±5.7	146±11	141±15	126±14	116±4	1 ± 0.5	2.3 ± 1.1	2.4 ± 1.4	3.7 ± 1.5
AZ91/5.0 wt.% rCF100	104±4	97±5	85±7.6	79±5.2	146±11	135±13	123±8	105±14	0.8 ± 0.2	1.2 ± 0.5	1.3 ± 0.5	1.3 ± 0.8
AZ91/5.0 wt.% rCF500	102±6	104±12	84±5.5	79±2.7	135±17	133±19	117±16	109±5.5	0.6 ± 0.2	1.2 ± 1	1.1 ± 0.6	1.2 ± 0.4

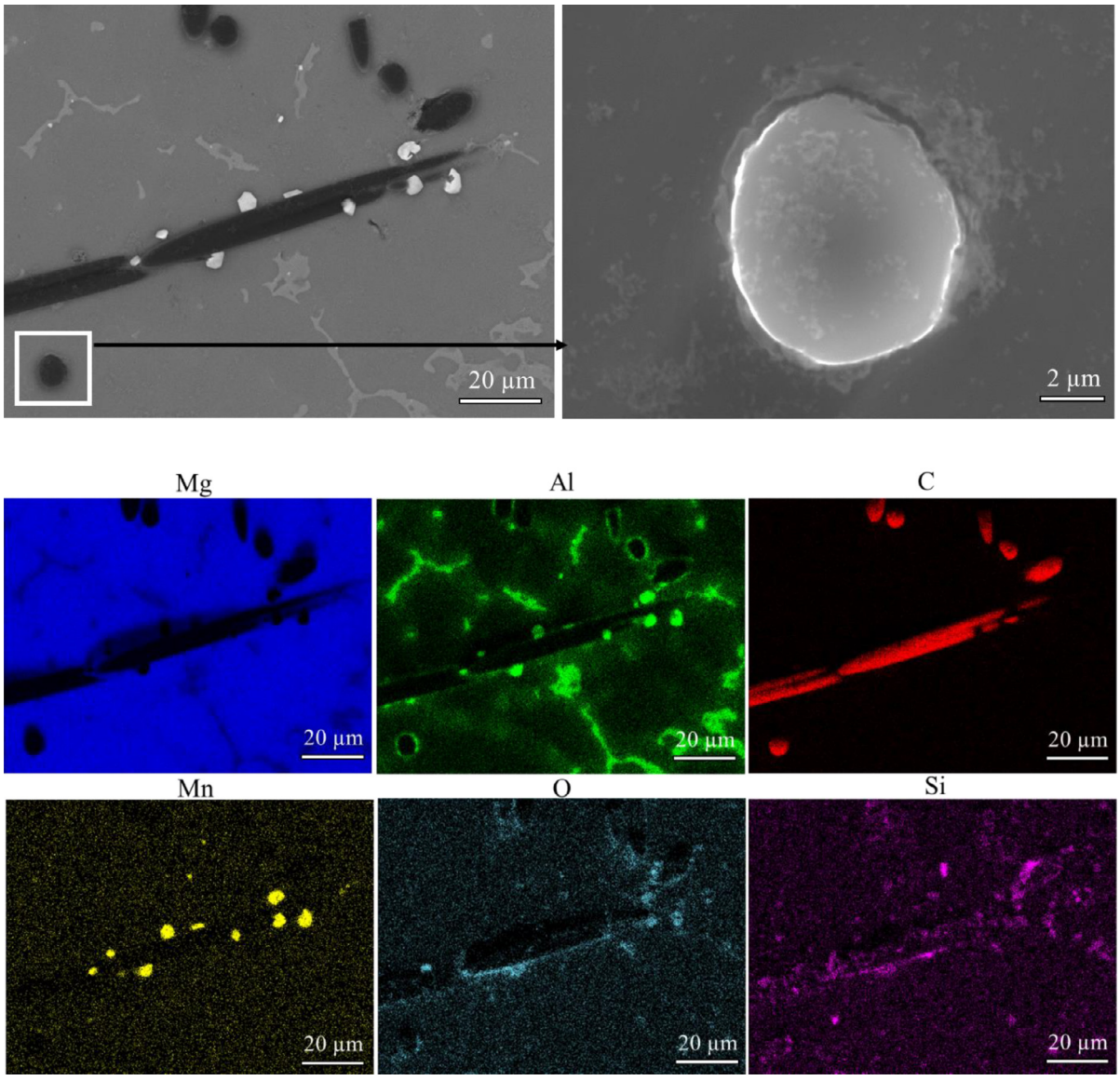

Fig. 6. EDX elemental mapping analysis on a selected area of AZ91/2.5 wt.%rCF100 composite.

Table 5
Compressive properties of cast AZ91 alloy and its composites reinforced with rCFs at different test temperatures.

	0.2% CPS (MPa)				UCS (MPa)				Failure strain (%)			
Sample/test temperature	RT	150 °C	175 °C	200 °C	RT	150 °C	175 °C	200 °C	RT	150 °C	175 °C	200 °C
AZ91	93 ± 3	89 ± 4	86 ± 1.3	81 ± 4	262 ± 7	264 ± 24	243 ± 14	225 ± 10	6.6 ± 1.7	8 ± 4	9 ± 1	24 ± 8
AZ91/2.5 wt.% rCF100	117 ± 4	110 ± 3	103 ± 1	101 ± 4	373 ± 10	355 ± 18	337 ± 40	260 ± 30	11 ± 0.8	25 ± 2	31 ± 8	40 ± 5
AZ91/2.5 wt.% rCF500	119 ± 7	105 ± 2	106 ± 3	99 ± 2	379 ± 5	385 ± 17	369 ± 47	312 ± 32	11 ± 0.2	29 ± 2	33 ± 6	42 ± 5
AZ91/5.0 wt.% rCF100	133 ± 4	121 ± 8	114 ± 5	113 ± 3	377 ± 2	356 ± 16	285 ± 10	271 ± 35	9.5 ± 0.2	21 ± 5	30 ± 3	41 ± 8
AZ91/5.0 wt.% rCF500	134 ± 5	125 ± 4	116 ± 2	111 ± 2	356 ± 12	336 ± 3	279 ± 11	235 ± 20	8.6 ± 0.8	20 ± 1	27 ± 3	35 ± 7

enhancement by 5 wt.% rCFs could be due to the presence of increased reinforcement content as the incorporation of more fibres inferring more clusters can induce large amounts of pores, which is already shown in Figs. 4 and 5e. On the other hand, the failure strain values of the composites containing 2.5 wt.% fibres were considerably higher than those of composites with 5 wt.% fibres at elevated temperatures. It has been suggested that larger reinforcement rich regions at higher reinforcement additions could result in concentrated strains due to impeded plastic deformation of the matrix. The reduced ductility at 5 wt.% rCF content can be therefore attributed to that strain localization leading to premature failure because of the modulus difference between the fibres and alloy [39]. When considering the influence of fibre length

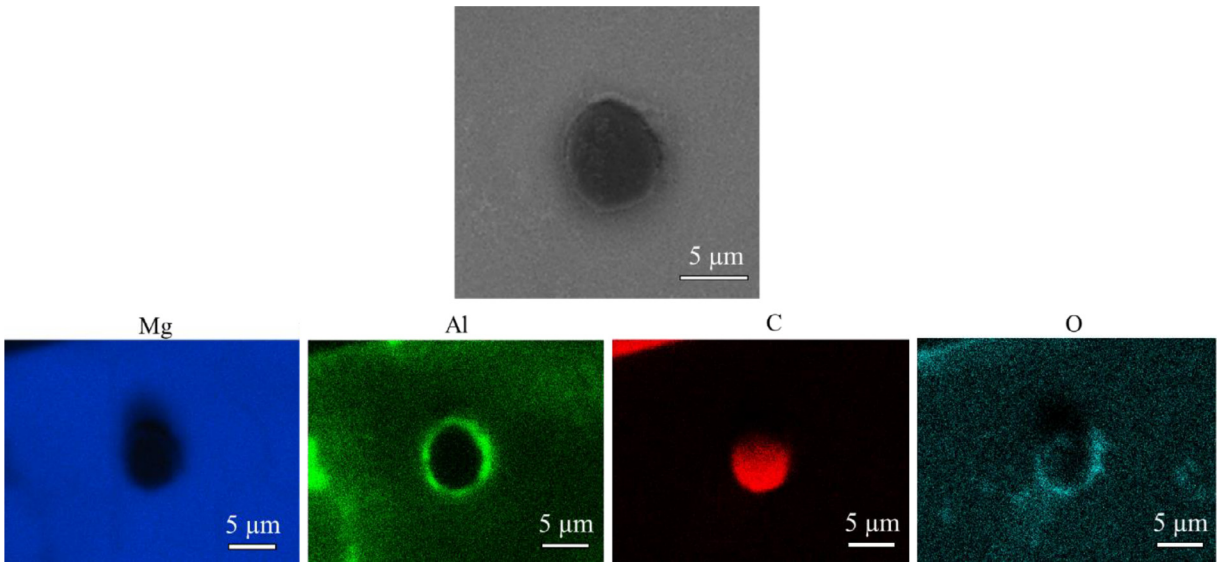

Fig. 7. EDX analysis of a single embedded rCF in the AZ91/2.5 wt.%rCF100 composite as indicated in Fig. 6.

on the tensile properties, it should be noted that there were no noticeable differences between the different rCF lengths used in terms of the observed composite microstructures due to the potential fibre breakage during the high shear dispersion (Fig. 5). Nevertheless, it is seen that the composite with 2.5 wt.% rCFs in 500 µm length generally displayed relatively higher strength and ductility results for the whole temperature range compared to those of the composites containing 2.5 wt.% fibres in 100 µm length. This can be ascribed to the reduced porosity level of AZ91/2.5 wt.%rCF500 composite in the first place (Fig. 4). In addition, Tian et al. [45] reported that fibre aspect ratio (fibre length/diameter) plays a crucial role along with the fibre orientation on the performance enhancement of Mg/CF composites and suggested that an aspect ratio up to around 20 can significantly contribute to the strength enhancement. When uneven orientations of rCFs into the composites are considered, in spite of the fibre breakage any difference between the average aspect ratios of rCFs (17 for 100 µm and 83 for 500 µm length, prior to the composite fabrication) is also likely to result in different tensile test outcomes. It is observed that the fibre length effect on the tensile properties of composites with 5 wt.% rCFs became less apparent than the composites with 2.5 wt.% rCFs as the results of AZ91/5.0 wt.% rCF100 and AZ91/5.0 wt.% rCF500 composites are very close to each other. This could be attributed to severe entanglement and clustering of CFs due to their relatively high concentration and it can be suggested that fibre length is unlikely to play a significant role above a certain reinforcement content leading to noticeable clustering.

The compressive proof stress (CPS) of AZ91 alloy was markedly improved about 27% and 43% with the incorporation of 2.5 and 5 wt.% rCFs, respectively, at ambient temperature. The similar improvement rates were also observed for the CPS of composites at elevated temperatures although all CPS values tend to drop. Apparently, the effect of fibre length on the CPS values (at a constant CF content) is not so remarkable through the whole temperature range. It is interesting that the axial PS values of all samples in compression are higher than those in tension. This asymmetry is often associated with the difference between tensile and compressive fibre axial stresses [46]. Contrary to the tensile properties, the UCS and compressive failure strain of rCF reinforced composites were enhanced compared to those of AZ91 alloy. RT UCS values of composites were approximately 43% higher than that of unreinforced reference alloy with only one exception as the AZ91/5.0 wt.% rCF500 composite showed approximately 35% improvement in the UCS. It is also seen in the UCS results that the strengthening effect induced by rCFs reduces as the testing temperature rises. RT ductility, compressive failure strain, of AZ91 alloy was enhanced with 2.5 wt.% rCF content by 67% and this enhancement decreased to around 44 and 30% for 5 wt.% rCF100 and rCF500 additions, respectively, due to cluster formation with increasing fibre content. Despite the fluctuations in the ductility values of all samples, maximum ductility enhancement by the incorporation of reinforcement was obtained at 150 and 175 °C. At 200 °C, the composites possessed comparable ductility increment with those tested at ambient conditions. Similar compressive ductility enhancement for Mg/SiC composites at both room and elevated temperature was reported by Rahmani et al. [47]. It is worth noting that materials having hexagonal crystal structure with a limited number of slip systems (hence limited ability to deform), such as Mg, are deformed by means of crystallographic slip and deformation twinning. Improved ductility of Mg matrix composites owing to reinforcement addition can be primarily linked to grain refinement, homogenously distributed reinforcement, and activation of non-basal slip mechanisms by texture changes [48,49]. Substantial grain refinement in the present study is more likely to be the main reason for the improved compressive ductility of composites.

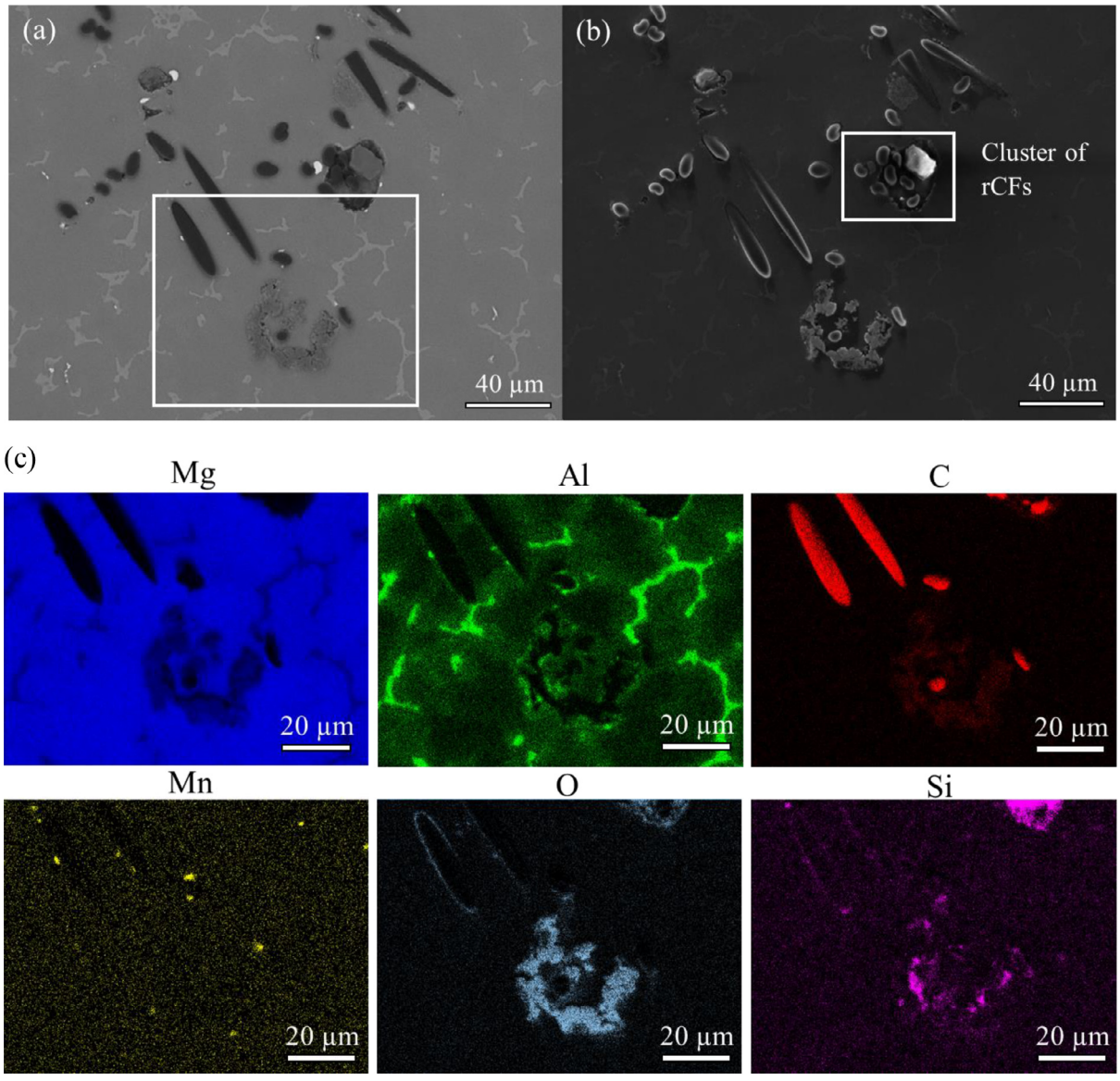

Fig. 8. (a) BSE and (b) SE SEM micrographs of the AZ91/2.5 wt.% rCF500 composite with (c) the EDX elemental mapping of a selected region.

It is also possible that local stresses induced by fibres and twins leading to intensification of non-basal slip during compression contribute to ductility enhancement [50]. However, further investigations based on detailed microstructural examination and grain orientation are required in order to ascertain the reasons for the compressive ductility enhancement. Moreover, compared to tensile plasticity, larger compressive failure strains of composites can be explained by the tendency of plastic deformation to take place early at the fibre ends as tensile deformation advances in the vicinity of the fibre ends [46]. Meanwhile, it is observed that the effects of fibre content and length on the UCS and compressive failure strain values are similar to those found in the tensile test results. It can be suggested that the AZ91/2.5 wt.% rCF500 sample is the most promising composite in terms of UCS and compressive ductility results.

In Fig. 12, the SEM tensile fracture surface images of AZ91 alloy and its composites reinforced with rCFs for all test temperatures are presented to understand the fracture mechanisms. While the fracture surfaces of AZ91 alloy without rCFs at RT (Fig. 12a) and 200 °C (Fig. 12p) revealed cleavage steps, those at 150 °C (Fig. 12f) and 175 °C (Fig. 12k) largely displayed dimples and tear ridges, which is more likely to indicate ductility improvement. This ductility improvement observed in the fracture surface analysis is also consistent with the tensile test data obtained (Table 4). Almost all composite fracture surfaces showed similar characteristic through the whole temperature range as they contain dimples and embedded rCFs in different orientations along with casting defects such as micropores (Fig. 12n and o). It can be suggested that the fracture of composites occurred via fibre breakage and fibre debonding depending the orientation

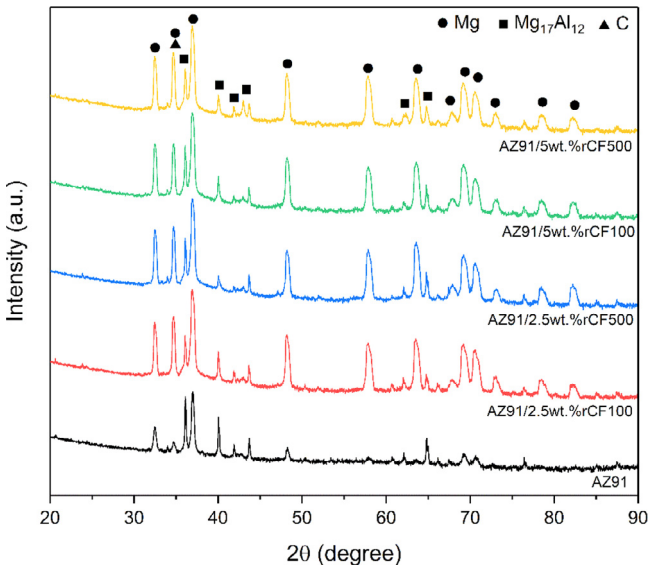

Fig. 9. (a) XRD peaks of the reference alloy and composites with rCFs.

of rCFs with respect to the tensile direction. For example, the fibre breakage can be observed at higher magnification in detail in Fig. 13a and b for the fibre clusters and individual fibre, respectively. Fig. 13c illustrates the fibre debonding where the rCFs were displaced from the matrix. The oxide rich intermediate layer, which was found on the surface of some rCFs embedded into AZ91 alloy in Fig. 7, was also observed on the fracture surfaces as indicated in Fig. 13d. In addition, the SEM fracture surface images of cast AZ91 alloy and its composites reinforced with rCFs after compression testing at RT are shown in Fig. 14 (Note that the fracture surface images after compression tests at elevated temperatures were not obtained because complete fracture did not occur resulting in two separate broken pieces due to the softening/mushing effect at that temperature range). AZ91 alloy displayed a typical flat cleavage fracture along with some cleavage steps and microcracks (Fig. 14a). However, the dimpled structures are more prominent in the fractographic images of composites without significant cracks (Fig. 14b–d, especially in Fig. 14c). This may imply that the compressive properties of composites were enhanced via the crack bridging effect of rCFs compared to those of the reference alloy. Nevertheless, further investigations are needed to fully understand the effect of rCFs on the fracture mechanism of AZ91 alloy at both room and elevated temperatures.

3.4. Creep

The investigated materials were tested with compression creep tests, because a compressive stress for magnesium alloys represents the typical load for applications. Most magnesium alloy components are produced by high-pressure die casting, gravity die casting or sand casting and then bolted together or to surrounding structures. During this process, the component is subjected to compressive stress, which can even increase with rising temperatures, e.g. if the screws are made of an aluminium alloy or steel. These materials have lower coefficients of thermal expansion (CTE) than the magnesium alloy, which generates additional compressive stresses in the components.

As examples, compressive creep curves taken at 150 °C and a constant stress of 80 MPa are shown in Fig. 15a. Fig. 15b shows the first derivative with respect to time of the same tests as plot of creep rates over time. The matrix alloy AZ91 shows primary creep followed by steady-state deformation and after about 70 h a transition to tertiary creep where the specimen fails. The rCF-reinforced AZ91 composites show significantly shorter primary creep and a very long stationary secondary creep range. From the curves in Fig. 15b, the minimum creep rates for the tests at 150 °C and 80 MPa are determined.

With the minimum creep rates for all stresses, graphs can be generated for the tests at 150 °C, 175 °C and 200 °C from which the stress exponent n can be determined. This follows the Norton equation, which shows the relationship between the minimum creep rate and the applied creep stress at constant temperature. Fig. 16a, b and c show these graphs.

It can be seen that at 150 °C all materials reinforced with rCFs have approximately the same creep resistance. The deviation of the individual minimum creep rates is only minor. The situation is different with the minimum creep rates of AZ91. At a creep stress of 60 MPa, the minimum creep rate is an order of magnitude smaller than that of the reinforced

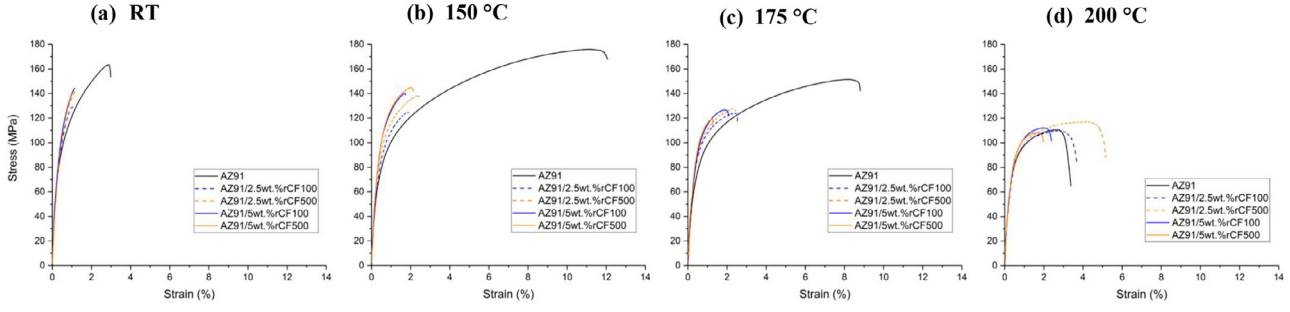

Fig. 10. Representative tensile engineering stress versus strain curves of cast AZ91 alloy and its composites reinforced with rCFs for (a) RT, (b) 150 °C, (c) 175 °C and (d) 200 °C.

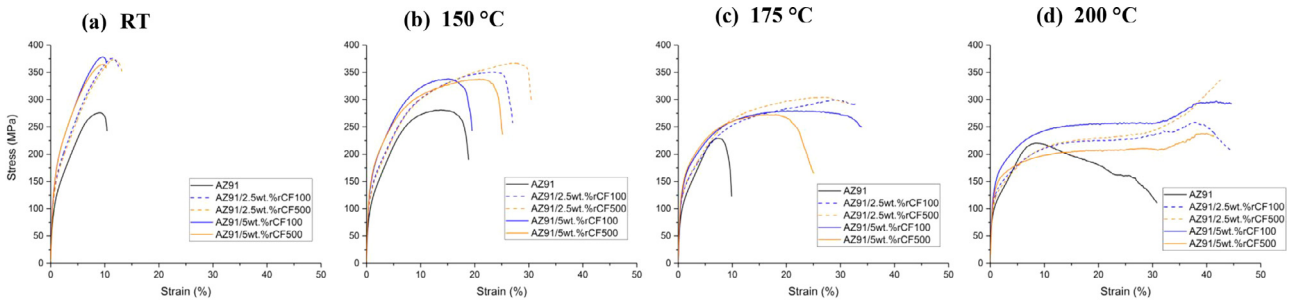

Fig. 11. Representative compressive engineering stress versus strain curves of cast AZ91 alloy and its composites reinforced with rCFs for (a) RT, (b) 150 °C, (c) 175 °C and (d) 200 °C.

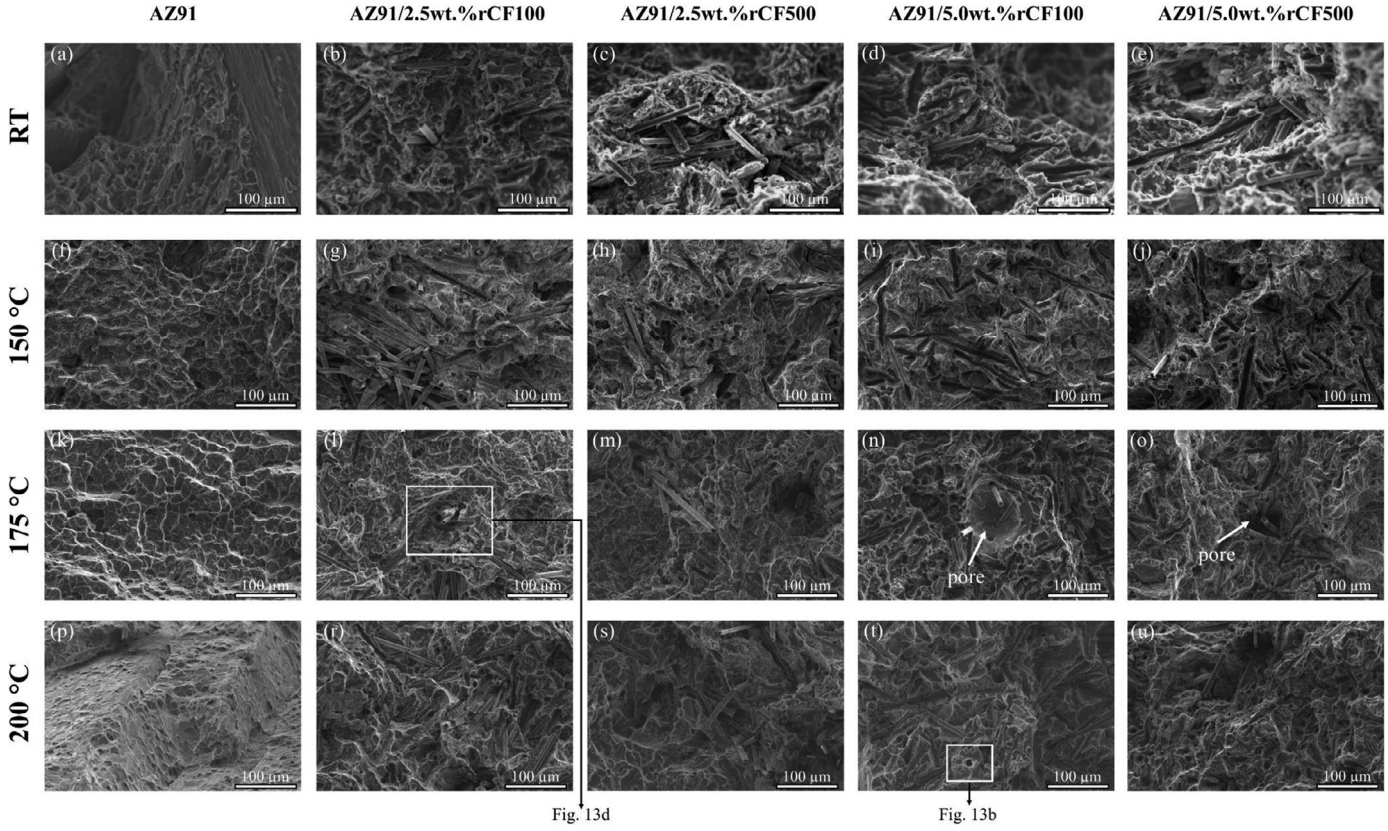

Fig. 12. Representative SEM fracture surface images of cast AZ91 alloy and its composites reinforced with rCFs after tensile testing at various temperatures.

AZ91. Comparable minimum creep rates for all materials can only be determined at stresses from 80 MPa upwards. For the reinforced AZ91, stress exponents can be determined by linear fits that range between 5.9 and 7.5. A linear fit is not possible for the pure AZ91, therefore a stress exponent cannot be determined.

It is similar with the plotting of minimum creep rate over creep stress in tests at 175 °C. Again, all reinforced AZ91-based composites show very similar minimum creep rates with stress exponents between 5.4 and 6.2, but the unreinforced AZ91 has significantly lower minimum creep rates at 60 and 80 MPa. Only at 100 MPa the creep rate is even slightly higher than that of the composites. A stress exponent of 17.4 can be calculated by applying a linear fit.

Minimum creep rates over applied stresses at 200 °C creep tests show again similar behaviour. Fibre reinforced AZ91 shows similar behaviour no matter what content and fibre length is used. Stress exponents are between 5.4 and 6.6. Unreinforced AZ91 has significantly lower minimum creep rates and a stress exponent of 9.3. The lower the applied stress, the larger is the difference between rCF reinforced composites and unreinforced AZ91.

The microstructure of AZ91 consists of α-magnesium and the β-phase $Mg_{17}Al_{12}$. This β-phase is mainly present at the grain boundaries and has a very low melting point of only 437 °C. It is responsible for only moderate creep properties of AZ91 when it is produced by high pressure die casting and

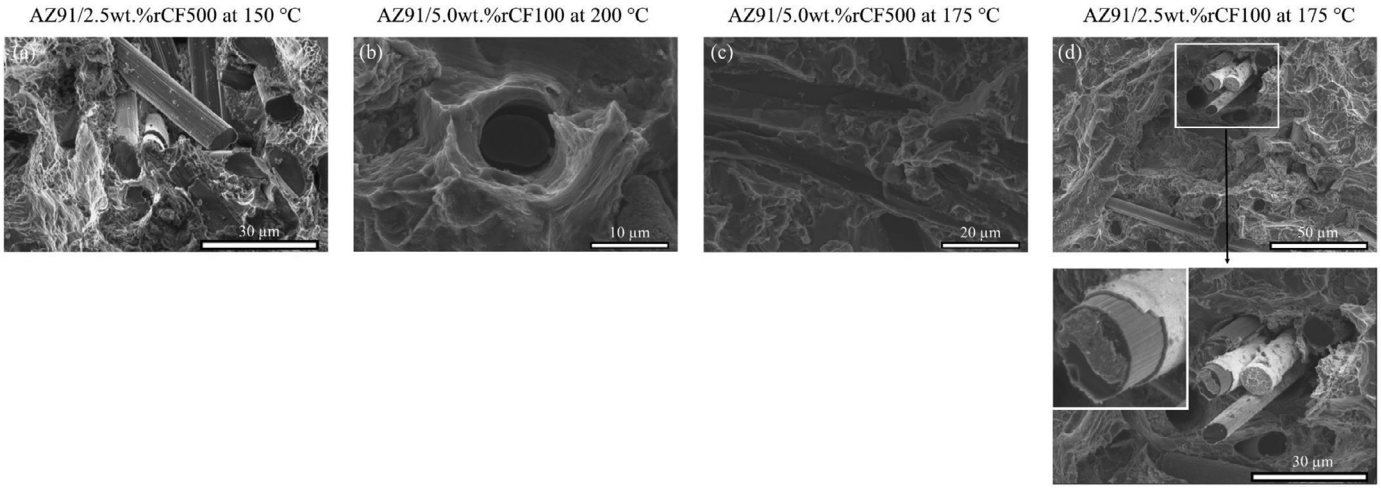

Fig. 13. Detailed SEM tensile fracture surface analyses of rCF reinforced AZ91 matrix composites showing (a) and (b) fibre breakage, (c) fibre debonding and (d) interlayer formed on the fibre surface.

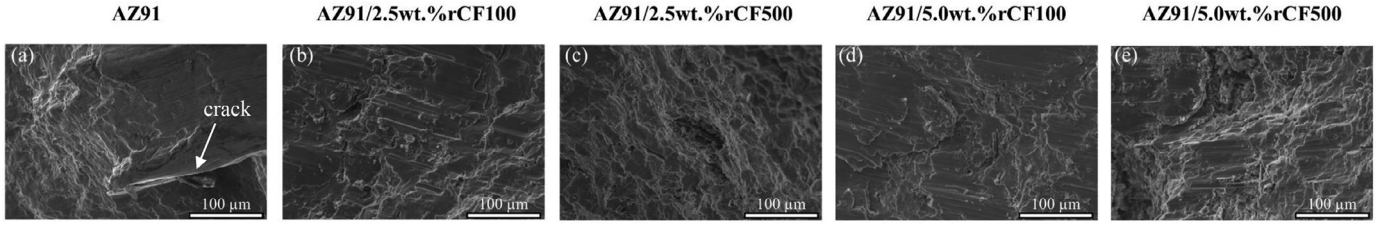

Fig. 14. Representative SEM fracture surface images of cast AZ91 alloy and its composites reinforced with rCFs after compression testing at RT.

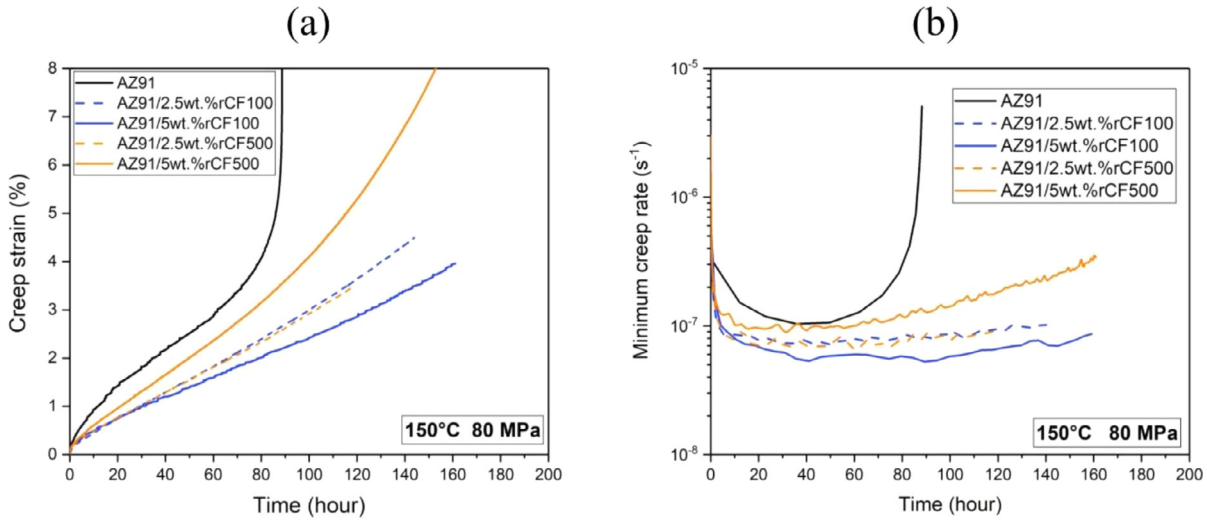

Fig. 15. (a) Creep deformation over time of compression creep tests performed at 150 °C and 80 MPa and (b) first derivative of (a) showing creep rate over time of identical tests.

a fine-grained structure is present, because the beta phase begins to soften at temperatures above 127 °C [5,6]. The finer the microstructure, the more β-phase is formed and the more grain boundary sliding can occur as a rate-controlling deformation mechanism during creep. The fact that the very fine-grained structure of the rCF-reinforced AZ91 creeps much faster than the coarse-grained unreinforced AZ91 is therefore due to the large difference in grain size, which cannot be compensated by the strength-enhancing influence of the rCF.

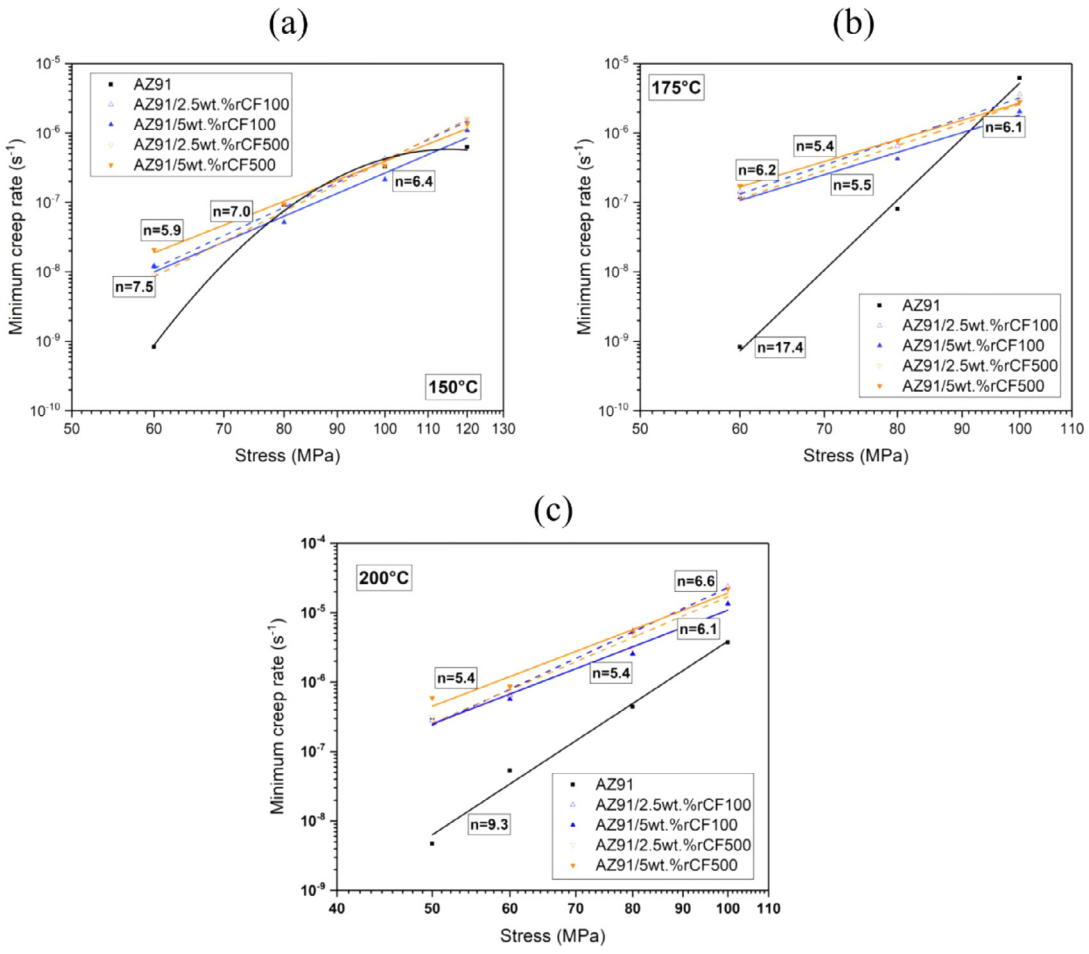

Fig. 16. Plots of minimum creep rate over applied creep stress at (a) 150 °C, (b) 175 °C and (c) 200 °C.

4. Conclusions

In summary, the following conclusions can be drawn from the conducted experiments.

1. The rCFs were successfully introduced into AZ91 alloy by means of a high shearing dispersion device. Reasonably uniform dispersion and distribution of rCFs were obtained with a few clusters. It was also found that the microstructure was refined and the porosity level increased with the addition of reinforcement.
2. Depending on the fibre length, i.e. 100 and 500 μm, the average hardness value of reference alloy was improved by approximately 6.5% and 13% with 2.5 and 5 wt.% rCF contents, respectively. Despite the divergent tensile test results, the composites usually have greater PS and decreased UTS and ductility for the temperature range between 25 and 200 °C compared to AZ91 alloy. The weakened properties were attributed to the porosity formation due to the relatively higher rCF content and the impaired load bearing capacity caused by the chemical attack between the reinforcement and matrix. Contrary to the tensile test outcomes, the UCS and compressive failure strain of composites were markedly enhanced, which was ascribed to the substantial grain refinement along with the activation of non-basal slip mechanisms by texture changes. Although the effects of fibre content and length on both tensile and compression properties were not found to be significant, AZ91/2.5 wt.% rCF500 composite generally displayed higher strength and ductility results for the entire temperature range as it has relatively higher fibre aspect ratio and lower rCF content inferring less agglomeration of reinforcement.
3. In general, for the cast recycled fibre reinforced composites, minimum creep rates were not improved in comparison to their unreinforced counterparts as a result of the significantly smaller grain sizes in the composites. The mechanism controlling creep was grain boundary sliding in the composites due to the increased amount of β phase formed at the grain boundaries.
4. The findings of this study are likely to be the first results performed on rCF reinforced Mg matrix composites and thus the processing parameters could be modified for future composite optimization. Therefore, future work is suggested to evaluate the full potential of such composites for high temperature engineering applications.

Acknowledgments

The authors would like to thank the German Academic Exchange Service (DAAD) for the scholarship provided to Dr. Sinan Kandemir during his stay at HZG to carry out this study. HZG and the Materials Research center at Izmir Institute of Technology are acknowledged for the provision of laboratory and SEM facilities, respectively. The authors would also like to thank CarboNXT GmbH (www.carbonxt.de) for providing the carbon fibres used in this study.

References

[1] I.J. Polmear, Light Alloys: Metallurgy of the Light Metals, Edward Arnold, London, 1981.
[2] B.B. Clow, Adv. Mater. Processes 150 (1996) 33–34.
[3] K.U. Kainer (Ed.), Magnesium – Alloys and Technology Wiley-VCH Verlag, 2003.
[4] H. Dieringa, J. Mater. Sci. 46 (2011) 289–306, doi:10.1007/s10853-010-5010-6.
[5] M. Regev, A. Rosen, M. Bamberger, Metall. Mater. Trans. A. 32 (2001) 1335–1345, doi:10.1007/s11661-001-0224-5.
[6] V. Sklenička, K. Kuchařová, M. Svoboda, I. Saxl, in: Proceedings of 12th International Conference on Fracture, Ottawa, 2009.
[7] H. Dieringa, Y. Huang, P. Wittke, M. Klein, F. Walther, M. Dikovits, C. Poletti, Mater. Sci. Eng., A. 585 (2013) 430–438, doi:10.1016/j.msea.2013.07.041.
[8] A.A. Luo, Int. Mater. Rev. 49 (2004) 13–30, doi:10.1179/095066004225010497.
[9] M. Pekguleryuz, M. Celikin, Int. Mater. Rev. 55 (2010) 197–217, doi:10.1179/095066010X12646898728327.
[10] S. Tekumalla, S. Seetharaman, A. Almajid, M. Gupta, Metals (Basel) 5 (2015) 1–39, doi:10.3390/met5010001.
[11] F. Aydin, Y. Sun, M.Emre Turan, J. Compos. Mater. 54 (2020) 141–152, doi:10.1177/0021998319860570.
[12] V. Sklenicka, M. Pahutova, K. Kucharova, M. Svaboda, T.J. Langdon, Key Eng. Mater. 171 (2000) 593–600, doi:10.4028/www.scientific.net/KEM.171-174.593.
[13] H. Dieringa, N. Hort, K.U. Kainer, Adv. Technol. Mater. Process. 6 (2004) 136–141.
[14] H.Z. Ye, X.Y. Liu, J. Mater. Sci. 20 (2004) 6153–6171, doi:10.1023/B:JMSC.0000043583.47148.31.
[15] H. Dieringa, N. Hort, Magnesium-based metal matrix nanocomposites—Processing and Properties, In: & Materials Society T. (eds) TMS 2018 147th Annual Meeting & Exhibition Supplemental Proceedings. The Minerals, Metals & Materials Series. Springer, Cham. 10.1007/978-3-319-72526-0_64.
[16] M.E. Turan, Y. Sun, F. Aydin, H. Zengin, Y. Turen, H. Ahlatci, Mater. Chem. Phys. 218 (2018) 182–188, doi:10.1016/j.matchemphys.2018.07.050.
[17] L. Chen, Y. Yao, Acta Metall. Sin. (English Letters). 27 (2014) 762–774, doi:10.1007/s40195-014-0161-0.
[18] L. Katsarou, M. Mounib, W. Lefebvre, S. Vorozhtsov, M. Pavese, C. Badini, J.M. Molina-Aldareguia, C.C. Jimenez, M.T.P. Prado, H. Dieringa, Mater. Sci. Eng., A. 659 (2016) 84–92, doi:10.1016/j.msea.2016.02.042.
[19] L. Ceschini, A. Dahle, M. Gupta, A.E.W. Jarfors, S. Jayalakshmi, A. Morri, S.Toschi F.Rotundo, R.A. Singh, Aluminum and Magnesium Metal Matrix Nanocomposites, Springer, Singapore, 2017, doi:10.1007/978-981-10-2681-2.
[20] http://ec.europa.eu/health/scientific_committees/opinions_layman/en/nanotechnologies/l-2/6-health-effects-nanoparticles.htm, (accessed 4 January 2020).
[21] S.J. Pickering, Compos. Part A. 37 (2006) 1206–1215, doi:10.1016/j.compositesa.2005.05.030.
[22] N. Perry, A. Bernard, F. Laroche, S. Pompidou, CIRP Ann.-Manuf. Technol. 61 (2012) 151–154, doi:10.1016/j.cirp.2012.03.081.
[23] G. Oliveux, L.O. Dandy, G.A. Leeke, Prog. Mater. Sci. 72 (2015) 61–99, doi:10.1016/j.pmatsci.2015.01.004.
[24] F. Meng, J. McKechnie, S.J. Pickering, Compos. Part A. 109 (2018) 207–220, doi:10.1016/j.compositesa.2018.03.011.
[25] M. Holmes, Reinf. Plast. 62 (2018) 148–153, doi:10.1016/j.repl.2017.11.012.
[26] A. Afrinaldi, T. Kakiuchi, S. Nakagawa, H. Moritomi, K. Kumabe, A. Nakai, A. Ohtani, Y. Mizutani, Y. Uematsu, Mater. Trans. 59 (2018) 475–481, doi:10.2320/matertrans.M2017297.
[27] K.A. Ajukumar, K.K.A. Kumar, K.K. Ravikumar, T.P.D. Rajan, U.T.S. Pillai, B.C. Pai, Mater. Sci. Forum. 710 (2012) 347–352, doi:10.4028/www.scientific.net/MSF.710.347.
[28] A. Feldhoff, E. Pippel, J. Woltersdorf, J. Microsc. 196 (1999) 185–193, doi:10.1046/j.1365-2818.1999.00618.x.
[29] K.U. Kainer, Development of magnesium-matrix composites for power train applications, in: Proceedings of the 12th International Committee on Composite Materials, Paris, 1999.
[30] B. Sommer, Untersuchung Zum Kriechverhalten der Kohlenstoffaserverstärkten Magnesiumlegierung AS41 PhD Thesis, TU Clauthal, 2000.
[31] A. Gryc, T. Rzychoń, Arch. Metall. Mater. 61 (2016) 1075–1081, doi:10.1515/amm-2016-0181.
[32] S. Tzamtzis, H. Zhang, N.Hari Babu, Z. Fan, Mater. Sci. Eng., A. 527 (2010) 2929–2934, doi:10.1016/j.msea.2010.01.013.
[33] X. Yang, Y. Huang, N.S. Barekar, S. Das, I.C. Stone, Z. Fan, Compos. Part A. 90 (2016) 349–358, doi:10.1016/j.compositesa.2016.07.025.
[34] H. Yang, Y. Huang, B. Song, K.U. Kainer, H. Dieringa, Mater. Sci. Eng., A. 755 (2019) 18–27, doi:10.1016/j.msea.2019.03.131.
[35] M. Song, G. Wu, W. Yang, W. Jia, Z. Xiu, G. Chen, J. Mater. Sci. Technol. 26 (2010) 931–935, doi:10.1016/S1005-0302(10)60150-8.
[36] T.J. Chen, Y. Ma, W.B. Lv, Y.D. Li, Y. Hao, J. Mater. Sci. 45 (2010) 6732–6738, doi:10.1007/s10853-010-4767-y.
[37] Y. Huang, K.U. Kainer, N. Hort, Scr. Mater. 64 (2011) 793–796, doi:10.1016/j.scriptamat.2011.01.005.
[38] M. Suresh, A. Srinivasan, U.T.S. Pillai, B.C. Pai, Procedia Eng 55 (2013) 93–97, doi:10.1016/j.proeng.2013.03.225.
[39] J. Liang, H. Li, L. Qi, W. Tian, X. Li, X. Chao, J. Wei, J. Alloys Compd. 728 (2017) 282–288, doi:10.1016/j.jallcom.2017.09.009.
[40] J.C. Viala, G. Claveyrolas, F. Bosselet, J. Bouix, J. Mater. Sci. 35 (2000) 1813–1825, doi:10.1023/A:1004745006226.
[41] A. Luo, Metall. Mater. Trans. A. 26 (1995) 2445–2455, doi:10.1007/BF02671259.
[42] S. Ugandhar, M. Gupta, S.K. Sinha, Compos. Struct. 72 (2006) 266–272, doi:10.1016/j.compstruct.2004.11.010.
[43] M.Y. Zheng, K. Wu, M. Liang. S. Kamado, Y. Kojima, Mater. Sci. Eng., A. 372 (2004) 66–74, doi:10.1016/j.msea.2003.09.085.
[44] Y.D. Huang, N. Hort, H. Dieringa, K.U. Kainer, Y.L. Liu, Acta Mater 53 (2005) 3913–3923, doi:10.1016/j.actamat.2005.04.039.
[45] W. Tian, L. Qi, J. Zhou, J. Guan, Comput. Mater. Sci. 89 (2014) 6–11, doi:10.1016/j.commatsci.2014.03.004.
[46] S. Trojanová, V. Gärtnerová, P. Lukáč, Z. Drozd, J. Alloys Compd. 378 (2004) 19–26, doi:10.1016/j.jallcom.2003.12.047.
[47] K. Rahmani, G.H. Majzoobi, A. Atrian, J. Compos. Mater. 54 (2020) 659–668, doi:10.1177/0021998319864629.
[48] H. Somekawa, T. Mukai, Scr. Mater. 53 (2005) 1059–1064, doi:10.1016/j.scriptamat.2005.07.001.
[49] S. Sankaranarayanan, M.K. Habibi, S. Jayalakshmi, K. Jia Ai, A. Almajid, M. Gupta, Mater. Sci. Technol. 31 (2015) 1122–1131, doi:10.1179/1743284714Y.0000000686.
[50] S. Ramezanzade, G.R. Ebrahimi, M. Torabi Parizi, H.R. Ezatpour, J. Compos. Mater. 54 (2020) 711–728, doi:10.1177/0021998319867464.